Progress In Electromagnetics Research C, Vol. 90, 79–93, 2019

Radar Scatter from Layered Media and Rough Surfaces

Pradeep Bobby* **and Eric W. Gill**

Abstract—The generalized function approach for modeling radio wave scattering has been used to develop expressions for the scatter from rough surfaces and for horizontally-stratified media. The scattered field from rough surfaces can be found in closed form if plane wave incidence is assumed, but the method is valid for any realizable source without resorting to using Hertz vectors. This approach was originally developed to model high frequency surface wave radar scattering from the ocean or across layers of ice covering the ocean using vertical polarization. This paper presents three extensions to the existing theory: the x component of the scattered field for rough surface scattering is developed, the assumption of a good conducting surface assumption is removed for a rough surface and the scatter from stratified media is simplified in terms of a scattering coefficient. The shape of the scattered field is not affected by the relative permittivity, but the intensity of the scattered field is weaker due to an increased transmission of energy through the surface. The goal for this research is to better understand how signatures from ice-penetrating radar can be used to distinguish hazardous ice ridges from other ice features. Here, ice ridges are modeled as layered media with a rough surface.

1. INTRODUCTION

There have been numerous approaches to model electromagnetic (EM) backscatter from rough surfaces and from horizontally stratified media, but these typically involve assumptions that limit the overall solutions to the point that the phenomena being modeled are not physically realizable. Lord Rayleigh [1] developed the perturbation method to study the reflection of acoustic waves from a sinusoidal surface and this was first extended to electromagnetic waves by Rice [2]. Rice considered static 2D rough surfaces that could be expressed as a Fourier Series with the series coefficients as random variables. The analysis was completed to second order for scatter from a perfectly conducting surface and a horizontally-polarized wave on a rough dielectric surface. Wait [3] considered reflection of a vertically-polarized EM wave from a 2D periodic surface using the Leontovich boundary conditions and derived results to second order. Barrick [4, 5] was interested in radar propagation across the ocean and considered the wave as being guided by a rough, conductive surface. The scattered field was limited to the component traveling away from the surface and multiple scattering was not included in the analysis. These results were extended to all spectral orders of scattering by Rosich and Wait [6]. Rodriguez and Kim [7] developed a unified perturbation expansion that reduced to Rice's results when the same assumptions are made, but the second order cross sections deteriorate as incidence angle or surface height increases. Perturbation methods are one of the most common approaches for modeling backscatter from rough surfaces. However they are only valid when the amplitude of surface roughness is much smaller than the radar wavelength and some implementations of the technique assume plane wave incidence.

Another frequently used approach to model rough surface scattering involves physical optics methods, commonly known as the Kirchoff or tangent plane approximation [8]. The surface fields are approximated by assuming the radius of curvature of the surface is much greater than the radar

Received 9 November 2018, Accepted 8 February 2019, Scheduled 20 February 2019
* Corresponding author: Pradeep Bobby (pbobby@mun.ca).
The authors are with the Memorial University of Newfoundland, Canada.

wavelength and the backscatter is modeled as coming from a tangent plane at each point on the surface. Unlike with perturbation theory, there is no restriction on the surface height, but the rate of change of surface variation is restricted and it is only valid for plane wave incidence and originally did not model multiple scatter.

Other rough surface scattering methods include the phase perturbation method [9], momentum transfer equation [10] and unified perturbation method [7]. The phase perturbation method applies a perturbation expansion to a parameter related to the complex phase and has been successfully employed in environments with moderate slope and curvature. The momentum transfer approach assumes a slightly rough surface in which the momentum transfer is small tangential to the surface compared to the momentum transfer perpendicular to the surface and the expansion is based on this parameter. The unified perturbation method is applicable for a wider range of surface slopes and heights.

Several approaches have been developed to model backscatter from stratified media. Wait [11] has developed very comprehensive equations for plane wave, spherical wave and cylindrical wave sources for homogeneous layers and layers where the permittivity follows a specific profile. Methods were also developed for backscatter from inhomogeneous layers using the Wentzel-Kramers-Brillouin (WKB) method. Tamir et al. [12] assumed the permittivity was sinusoidally varying in the vertical direction and was able to obtain analytical results for the scatter. Chen [13] considered scatter from stratified media where there was a small amount of randomness with specific profiles and recommended using additional layers if the inhomogeneity due to randomness was too large. Bahar [14] used a full wave technique in the analysis of stratified media.

Walsh [15–18] developed an analysis procedure that may be applied to rough surface and stratified media backscatter. The method is based on 'generalized functions' and uses Green's functions. For the rough surface, two integral equations are generated that describe the fields above and below the surface along with a boundary equation that naturally evolves from the analysis. Unlike perturbation theory and the tangent plane approximation the only assumptions are that the surface is bounded, the electrical conductivity σ, magnetic permeability μ and dielectric permittivity ϵ are fixed for the half space above the surface and for the half space below the surface and that the source and scattered fields are bandlimited such that $k_x^2 + k_y^2 < k^2$, where k_x and k_y are the spatial transform variables and k is the radar wavenumber in free space. Another assumption made is that the electric field is constant for a localized region of the rough surface. This approach may be used to model backscatter from realistically rough surfaces using general sources.

Walsh's approach yields closed form solutions for rough surface backscatter when plane wave incidence is assumed, but the scattered fields for any realizable source can be found numerically. In Section 2 it is shown that Walsh's method can be used to develop the scattering equations for a horizontal dipole over a rough surface. The x component of the electric field has been derived, unlike in the original work where the y and z components alone were presented. The equations have been modified to include the case where the dielectric permittivity of the surface is arbitrary, thus removing the assumption of a good conducting surface and allowing Walsh's method to be applied to more general rough surfaces. The equations for stratified media backscatter are outlined in Section 3. The field above the layers has a direct wave and a reflected component, similar to the rough surface case. One of the terms in the scattering is negligible, which makes it possible to express the scattering from stratified media using a reflection coefficient. A justification for modeling ice ridges as a rough surface over layers is provided in Section 4.

2. ROUGH SURFACE SCATTERING BACKGROUND

The rough surface scattering equations begin with Maxwell's equations, with the details leading to (1) below being found in [18]. The surface is bounded, i.e., $|f(x, y)| < C$ for some constant C and has mean height $z = 0$. The upper, semi-infinite half-space contains the source which, for convenience, is assumed to be free space. The lower, semi-infinite half-space is also homogeneous and distinct from free space. The Heaviside function is used to distinguish the fields and quantities above and below the surface such that $h(z - f(x, y)) = 1$ above the surface and zero otherwise. This geometry is illustrated in Figure 1.

The partial differential equation for the electric field can be determined by simplifying the terms for $\nabla \times \nabla \times \vec{E}$. The expression uses the following notations: γ_0 is the overall propagation constant; n_0

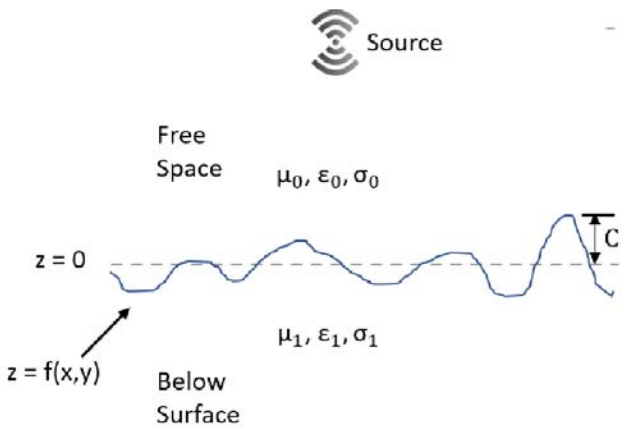

Figure 1. Illustration of rough surface geometry.

is the refractive index, which is the square root of the relative dielectric permittivity; T_{SE} is the electric source operator defined by $T_{SE} = \frac{1}{j\omega\epsilon_0}[\nabla(\nabla\cdot) + k^2]$; $\vec{J}_s$ is the current density; δ is the standard delta function; $\vec{n}$ is the normal vector to the rough surface; ω is the radar frequency; and ϵ_0 is the permittivity of free space. The electric field [18] is then governed by

$$\nabla^2\vec{E} + \gamma_0^2\vec{E} = \frac{n_0^2 - 1}{n_0^2}\nabla[\vec{n}\cdot\vec{E}^+\delta(z-f)] - T_{SE}(\vec{J}_s) \tag{1}$$

where $\vec{E}^+$ is the electric field just above the surface. This equation is further simplified by examining the x, y and z components of the electric field above and below the surface. Expressions for the Laplacian of the electric field above and below the surface are determined, leading to a set of three conditions that must be satisfied by the electric field:

$$\begin{aligned} h[\nabla^2(\vec{E}) + k^2\vec{E}] &= -T_{SE}(\vec{J}_s) \\ (1-h)[\nabla^2(\vec{E}) + \gamma^2\vec{E}] &= 0 \end{aligned} \tag{2}$$

$$\begin{aligned} &|\vec{n}|\left[\frac{\partial\vec{E}^+}{\partial n} - \frac{\partial\vec{E}^-}{\partial n}\right]\delta(z-f) + \nabla\cdot[\vec{n}(E_x^+ - E_x^-)\delta(z-f)\hat{x}] + \nabla\cdot[\vec{n}(E_y^+ - E_y^-)\delta(z-f)\hat{y}] \\ &+ \nabla\cdot[\vec{n}(E_z^+ - E_z^-)\delta(z-f)\hat{z}] = \frac{n_0^2-1}{n_0^2}\nabla[\vec{n}\cdot\vec{E}^+\delta(z-f)] = (n_0^2-1)\nabla[\vec{n}\cdot\vec{E}^-\delta(z-f)] \end{aligned} \tag{3}$$

where E_x^-, E_y^- and E_z^- are the components of the electric field just below the surface. These partial differential equations may be converted to integral equations by convolving with Green's functions, $K_{01}(x,y,z) = \frac{e^{-jkr}}{4\pi r}$, and $K_{02}(x,y,z) = \frac{e^{-j\gamma r}}{4\pi r}$ above and below the surface, respectively, where r is the position vector from the surface to the source. The three equations of Eqs. (2) and (3) may be expressed in a form to solve for the fields above the surface such that the only unknowns are $\frac{\partial\vec{E}^+}{\partial n}$, $\frac{\partial\vec{E}^-}{\partial n}$, $\vec{E}^+$ and $\vec{E}^-$.

Due to the convolution nature of the equations, they can be simplified through a two dimensional (x,y) spatial Fourier transform. The resulting integral equations, as given by

$$\int_{x'}\int_{y'}\left[\vec{G}(x',y') + \frac{\vec{F}(x',y')}{u_1}\right]e^{f(x',y')u_1}e^{-jk_xx'-jk_yy'}dy'dx' = 0 \tag{4}$$

$$2\underline{\vec{E}}_s^{z-}e^{-z^-u} = \int_{x'}\int_{y'}\left[|\vec{n}|^2\vec{E}^+ - \frac{\vec{R}^+}{u}\right]e^{-f(x',y')u}e^{-jk_xx'-jk_yy'}dy'dx' \tag{5}$$

are used to solve for the electric field. Here, $\underline{\vec{E}}_s^{z^-}$ is the two dimensional transform of the source electric field in the plane $z = z^-$ below the surface. The primed variables are introduced from the convolution and the underbar indicates Fourier transform variables. The remaining expressions are defined as $\vec{G}(x', y') = |\vec{n}|^2\vec{E}^+ - \frac{n_0^2-1}{n_0^2}(\vec{n}\cdot\vec{E}^+)\vec{n}$, $\vec{F}(x', y') = \vec{R}^+ + \frac{n_0^2-1}{n_0^2}\nabla_{xy}(\vec{n}\cdot\vec{E}^+)$, $\vec{R}^+ = -\frac{n_0^2-1}{n_0^2}\nabla_{xy}(\vec{n}\cdot\vec{E}^+) - u_1\left[|\vec{n}|^2\vec{E}^+ - \frac{n_0^2-1}{n_0^2}(\vec{n}\cdot\vec{E}^+)\vec{n}\right]$, $u_1 = \sqrt{\lambda^2 - n_0^2k^2}$, $u = \sqrt{\lambda^2 - k^2}$ and $\lambda = \sqrt{k_x^2 + k_y^2}$. Solving the integral equations of Eqs. (4) and (5) make it possible to solve for the scattered field using Eq. (2).

Walsh [18] was primarily interested in high frequency (HF) propagation across the ocean and was able to assume large n_0. Considering the original expression for u_1, this implies $|\lambda/k|^2 \ll |n_0|^2$. This assumption also implies that the integral equations of Eqs. (4) and (5) are spatially bandlimited.

2.1. Rough Surface Theory Extension

The extension of Walsh's method towards general, non-conducting surfaces begins with Eq. (4) where the expression for u_1 is retained instead of the simplification $u_1 \approx jkn_0$. This provides more general expressions than [18], but the scattered fields are still assumed to be bandlimited and the refractive index of the lower half-space is arbitrary (see Figure 1). Since the source has not been constrained, a reasonable choice of a finite current source that completely lies in the positive half space can be used. Thus, the source can also be taken to be spatially bandlimited. A closer look at Eq. (5) shows that the term $e^{-f(x',y')u}$ is present in the integral indicating that when k_x, k_y are large, the integrand will be small even when the relative permittivity is small. This makes it possible to retain the assumption of a spatially bandlimited solution with an arbitrary refractive index. To explicitly express that the bandwidth is restricted to low frequencies the exponential will be denoted with a subscript L as $e_L^{-f(x',y')u}$.

Without loss of generality for an electrically large surface it is possible to assume that the surface roughness $f(x, y)$ is periodic and can be expressed as a Fourier series. Fortunately it is sufficient to consider the surface to be much larger than a wavelength to assume a rough periodic surface [19]. Thus, $e_L^{-f(x',y')(u'-u)}$ will also be periodic. For a completely random rough surface, the Fourier series coefficients can be taken as random variables and the period can extend to infinity [20]. Although this method is valid for random rough surfaces, a simple 1D sinusoidal surface will be used to illustrate the technique through simplified notation. The scattering equations for a specific surface, say $f(x, y) = b + a\cos(k_0y)$ can be found from Eq. (5). We note that $\vec{n} = -f_x\hat{x} - f_y\hat{y} + \hat{z}$ where $f_x = \frac{\partial f}{\partial x}$ and $f_y = \frac{\partial f}{\partial y}$ and use this to expand $\vec{R^+}$ in Eq. (5). Since we have assumed a surface that varies in the y dimension only, the equations are simplified as all surface derivatives with respect to x are zero. The equations are solved for each of the x, y and z components separately. The original research [15] developed the y and z components of the fields and through the current research the x components of the field have been derived and are presented here. The simulations will be based on the y and z components of the field since the surface has been assumed to only have variation in the y direction and the x component of the field does not illustrate the impact of generalizing the refractive index of the surface.

Using the simplified surface, the expression for R_x^+ reduces to become

$$R_x^+ = -\frac{n_0^2 - 1}{n_0^2}\left[-f_y\frac{\partial E_y^+}{\partial x} + \frac{\partial E_z^+}{\partial x}\right] - u_1[(1 + f_y^2)E_x^+]\frac{\partial E_y^+}{\partial x}. \tag{6}$$

Substituting this expression into Eq. (5) yields

$$\begin{aligned} 2u\underline{E}_s x^{z^-}e^{-z^-u} = {} & (u + u_1)\int_{y'}\int_{x'} E_x^+K_L dx'dy' + (u + u_1)\int_{y'}\int_{x'} f_y^2E_x^+K_L dx'dy' \\ & - \frac{n_0^2 - 1}{n_0^2}\int_{y'}\int_{x'}\frac{\partial E_y^+}{\partial x}K_L dx'dy' + \frac{n_0^2 - 1}{n_0^2}\int_{y'}\int_{x'}\frac{\partial E_z^+}{\partial x}K_L dx'dy' \end{aligned} \tag{7}$$

where $K_L(x', y', k_x, k_y) = e_L^{-f(x',y')u}e^{-jk_xx'-jk_yy'}$. The expressions for the y and z components are similar.

Rather than searching for the complete solution, the objective will be to solve for the bandlimited case, referred to as the principal solution. Each component of the electric field may be expressed as the inverse Fourier transform of a function, $\underline{G}_1$. For example,

$$E_x^+(x',y') = \frac{1}{4\pi^2}\int_{k_{y'}}\int_{k_{x'}} \underline{G}_{1x}(k'_x,k'_y) e_L^{-f(x',y')u'} e^{-jk_x x' - jk_y y'} dx'dy'. \tag{8}$$

Solving for the electric field above the surface is simplified to solving for G_1. In solving each integral of Eq. (7), the factor $e_L^{-f(x',y')(u'-u)}$ can be expressed in terms of a Fourier series as

$$e_L^{-f(x',y')u} = \sum_n A_n(u'-u)e^{jnk_0y'}. \tag{9}$$

The A_n terms are the Fourier coefficients, which can be found in the standard manner. After some algebra, Eq. (7) is simplified to

$$\begin{aligned} 2\underline{E}_{sx}^{z^-} e^{-z^-u} u =& \sum_q \left\{ A_q(u_q-u)\left[(u+u_1)\left(1+\frac{(aK_0)^2}{2}\right)\right] - \frac{(aK_0)^2}{4}(u+u_1)\cdot \right. \\ & \left. [A_{q+2}(u_q-u)+A_{q-2}(u_q-u)] \right\} G_{1x}(k_x,k_y-qK_0) \\ & + \sum_q \left(\frac{n_0^2-1}{n_0^2}\right)\left(\frac{aK_0}{2}\right)[A_{q-1}(u_q-u)-A_{q+1}(u_q-u)]\, G_{1y}(k_x,k_y-qK_0) \\ & + \sum_q \left(\frac{n_0^2-1}{n_0^2}\right)(jk_x)A_q(u_q-u)G_{1z}(k_x,k_y-qK_0). \end{aligned} \tag{10}$$

In general for a rough surface, the summations of Eq. (10) may extend to infinity. However, for the bandlimited solution they are constrained by $k_x^2+(k_y-qk_0)^2 \le k^2$. A similar process can be followed to derive the expression for the scattered field as

$$\begin{aligned} \underline{E}_x^s =& \frac{e^{-z^+u}}{2u}\left[\sum \left\{ \left[(u-u_1)(1+\frac{(aK_0)^2}{2})\right] A_q(u_q+u) - (u-u_1)\left(\frac{(aK_0)^2}{4}\right)\cdot \right.\right. \\ & \left. [A_{q-2}(u_q+u)+A_{q+2}(u_q+u)] \right\} G_{1x}(k_x,k_y-qK_0) \\ & + \sum_q \left\{ \left(-\frac{n_0^2-1}{n_0^2}\right)\frac{aK_0}{2}[A_{q-1}(u_q+u)-A_{q+1}(u_q+u)]\, G_{1y}(k_x,k_y-qK_0) \right. \\ & \left.\left. + \sum_q \left\{ \left(-\frac{n_0^2-1}{n_0^2}\right) jk_x A_q(u_q+u) \right\} G_{1z}(k_x,k_y-qK_0) \right]. \end{aligned} \tag{11}$$

The expressions for the y and z components of the source and scattered fields are derived in the same fashion and have a similar structure to the equations for the x component provided. The summation over q is interpreted to include all the modes of the source field. It can be shown that $A_q(0)=1$ when $q=0$ and is zero otherwise. By taking the $q=0$ term out of the summations, the expressions may be reorganized in the form, for example,

$$\underline{E}_{sx} = (I+T)G_{1x} \tag{12}$$

where I is the identity operator, and T includes the summation terms for $q \neq 0$. A Neuman series expansion, $(I+T)^{-1} = I - T + T^2 - T^3 + \ldots$, can be used to solve for G_1. This allows the expression for each component of G_1 to be expressed as a matrix equation. For the simple 1D surface discussed here, the y and z component equations are coupled and are not dependent on the x component, but the full general equation may be given as

$$\begin{bmatrix} \underline{E}_s^x \\ \underline{E}_s^y \\ \underline{E}_s^z \end{bmatrix} = \begin{bmatrix} \alpha & \beta & \gamma \\ \delta & \epsilon & \zeta \\ \eta & \theta & \iota \end{bmatrix} \begin{bmatrix} \underline{G}_{1x} \\ \underline{G}_{1y} \\ \underline{G}_{1z} \end{bmatrix}. \tag{13}$$

The elements α, β and γ in the first matrix on the right hand side of Eq. (13) are the multipliers on $\underline{G}_{1x}$, $\underline{G}_{1y}$, $\underline{G}_{1z}$ from Eq. (10). Similarly, the remaining two rows of that matrix correspond to the multipliers on the components of $\underline{G}_1$ for the y and z components of the source field. For the chosen surface, both $\delta = \eta = 0$. Since the source terms will be known in Eq. (13), matrix inversion yields the unknown G_1 terms. Expressions for the scattered fields can then be written, and the x component, provided for illustration, is

$$\underline{E}_x^s = \frac{e^{-z^+u}}{2u}\left[(u-u_1)\left(1+\frac{(aK_0)^2}{2}\right)\right]\begin{bmatrix}\underline{G}_{1x}\\ \underline{G}_{1y}\\ \underline{G}_{1z}\end{bmatrix}^T\begin{bmatrix}\underline{\rho}\\ \underline{\sigma}\\ \underline{\tau}\end{bmatrix}. \tag{14}$$

Here ρ, σ and τ are the respective multipliers on $\underline{G}_{1x}, \underline{G}_{1y}, \underline{G}_{1z}$ from Eq. (11), and similar expressions can be found for the y and z components of the scattered fields. Using Eq. (13) it is possible to express the x component of the scattered field in terms of the source as

$$\underline{E}_x^s = \frac{e^{-z^+u}}{2u}\left[(u-u_1)\left(1+\frac{(aK_0)^2}{2}\right)\right]\begin{bmatrix}\underline{E}_s^x\\ \underline{E}_s^y\\ \underline{E}_s^z\end{bmatrix}^T\left(\begin{bmatrix}\alpha & \beta & \gamma\\ \delta & \epsilon & \zeta\\ \eta & \theta & \iota\end{bmatrix}^T\right)^{-1}\begin{bmatrix}\underline{\rho}\\ \underline{\sigma}\\ \underline{\tau}\end{bmatrix}. \tag{15}$$

For calculation purposes, it is more convenient to express Eq. (15) in terms of $(\underline{E}_{sx})^q e^{-z^-}$, $(\underline{E}_{sy})^q e^{-z^-}$ and $(\underline{E}_{sz})^q e^{-z^-}$, which are the modes of the source below the surface at $z = z^-$ and the source terms are

$$\begin{aligned}
(\underline{E}_{sx})^q &= e^{-z^+u}\sum_{q=q^-}^{q^+}\frac{2(\underline{E}_{sx}^{z^-}e^{-z^-u})u_q}{(u+u_{1q})\left(1+\frac{(ak_0)^2}{2}\right)}\\
(\underline{E}_{sy})^q &= e^{-z^+u}\sum_{q=q^-}^{q^+}\frac{2(\underline{E}_{sy}^{z^-}e^{-z^-u})u_q}{(u_q+u_{1q})\left[1+\frac{(ak_0)^2}{2}\frac{1}{n_0^2}\right]}\\
(\underline{E}_{sz})^q &= e^{-z^+u}\sum_{q=q^-}^{q^+}\frac{2(\underline{E}_{sz}^{z^-}e^{-z^-u})u_q}{u_q+\frac{u_{1q}}{n_0^2}+\frac{(ak_0)^2}{2}(u_q+u_1)}.
\end{aligned} \tag{16}$$

The x-component of the scattered field expressed as modes of the source may be written as

$$\begin{aligned}
\underline{E}_x^s =& e^{-z^+u}\sum_{q=q^-}^{q^+}\left[\frac{(u-u_1)\left(1+\frac{(aK_0)^2}{2}\right)}{(u_q+u_{1q})\left(1+\frac{(ak_0)^2}{2}\right)}\right]\frac{u_q}{u}T_q^x(k_x,k_y)(\underline{E}_{sx}^{z^-}e^{-z^-u})^q\\
&+e^{-z^+u}\sum_{q=q^-}^{q^+}\left[\frac{(u-u_1)\left(1+\frac{(aK_0)^2}{2}\right)}{(u_q+u_{1q})\left[1+\frac{(ak_0)^2}{2}\frac{1}{n_0^2}\right]}\right]\frac{u_q}{u}T_q^y(k_x,k_y)(\underline{E}_{sy}^{z^-}e^{-z^-u})^q\\
&+e^{-z^+u}\sum_{q=q^-}^{q^+}\left[\frac{(u-u_1)\left(1+\frac{(aK_0)^2}{2}\right)}{u_q+\frac{u_{1q}}{n_0^2}+\frac{(ak_0)^2}{2}(u_q+u_{1q})}\right]\frac{u_q}{u}T_q^z(k_x,k_y)(\underline{E}_{sz}^{z^-}e^{-z^-u})^q
\end{aligned} \tag{17}$$

where T_q is the multiplication of the last two matrices of Eq. (15). The scattered field may be expressed in terms of scattering coefficients as

$$\underline{E}_x^s = \frac{e^{-z^+u}}{2u}\left[\sum_q s_{xx}G_{1x}(k_x,k_y-qK_0)+\sum_q s_{xy}G_{1y}(k_x,k_y-qK_0)+\sum_q s_{xz}G_{1z}(k_x,k_y-qK_0)\right]. \tag{18}$$

The definitions of the scattering coefficients given by s_{xx}, s_{xy} and s_{xz} are apparent from Eq. (11) and are in terms of the modes of the source. The copolarized component of the scatter is indicated by s_{xx} and the depolarized portions of the signal are represented by s_{xy} and s_{xz}. These scattering coefficients indicate the proportion of the scattered field from the surface in each direction and the sum of the scattering coefficients indicates the total proportion of scattered energy. Expression (17) is an extension of past results in that it applies to general non-conducting surfaces.

2.2. Rough Surface Scatter Results

Sample results for the y and z components of the field are shown for the case when the source is an uniform plane wave with a y component only as results are easier to interpret, especially for a simple 1D sinusoidal surface. The incident wave is

$$\vec{E}_s = E_{0y} e^{-jk_x^0 x - jk_y^0 y + u^0 z} \hat{y} \tag{19}$$

where $k_x^0 = k\cos\theta_x$, $k_y^0 = k\cos\theta_y$ and $u^0 = \sqrt{(-k_x^0)^2 - (-k_y^0)^2 - k^2}$. The angles θ_x and θ_y are measured from the source to the x and y axes, respectively. For a plane wave at nadir incidence, as considered here, $\theta_x = \theta_y = \pi/2$. The 2D (x, y) Fourier transform of the source is

$$\underline{E}_{sy} = 4\pi^2 E_{0y} e^{u_0 z} \delta(k_x + k_x^0)\delta(k_y + k_y^0). \tag{20}$$

Due to the delta functions in Eq. (20) and the corresponding expression for $\underline{E}_{sz}$ it is possible to conduct the inverse Fourier transform of Eq. (17) in closed form to yield the scattered field for plane wave at normal incidence as

$$\begin{aligned} E_y^s =& E_{0y} \sum_{q=q^-}^{q=q^+} \left[\frac{u_q^0 - u_{1q}^0 + \dfrac{(aK_0)^2}{2}\left(u_q^0 \dfrac{2n_0^2 - 1}{n_0^2} - \dfrac{u_{1q}^0}{n_0^2} \right)}{(u^0 + u_1^0)\left(1 + \dfrac{(aK_0)^2}{2n_0^2} \right)} \right] \frac{u^0}{u_q^0} \cdot \\ & T_q^y[-k_x^0, -(k_y^0 - qK_0)] e^{-jk_x^0 x - j(k_y^0 - qK_0)y - u_q^0 z^+} \\ & + E_{0z} \sum_{q=q^-}^{q=q^+} \left[\frac{u_q^0 - u_{1q}^0 + \dfrac{(aK_0)^2}{2}\left(u_q^0 \dfrac{2n_0^2 - 1}{n_0^2} - \dfrac{u_{1q}^0}{n_0^2} \right)}{\left(u_0 + \dfrac{u_1^0}{n_0^2} \right)\left(1 + \dfrac{(aK_0)^2}{2}(u_0 + u_1^0) \right)} \right] \frac{u^0}{u_q^0} \cdot \\ & T_q^z[-k_x^0, -(k_y^0 - qK_0)] e^{-jk_x^0 x - j(k_y^0 - qK_0)y - u_q^0 z^+}. \end{aligned} \tag{21}$$

The geometry of the problem is shown in Figure 1. Figure 2(a) shows a simulation of Walsh's original results when a high permittivity is assumed and Figure 2 shows the results when the refractive index is 1.8, a value commensurate with freshwater ice.

It can be seen that the shapes of the scattered field are the same in both cases, but the field strength is lower when the permittivity is lower. This result is intuitive since an infinite permittivity results in complete reflection/scattering of the incident energy and as the permittivity of the surface lowers an increasing portion of the energy will be transmitted through the medium. It is possible to verify the amount of scattered and transmitted field using the Fresnel reflection coefficient for normal incidence as given in Eq. (22)

$$\Gamma = \frac{n_1 - n_2}{n_1 + n_2}, \tag{22}$$

where $n_1 = \sqrt{\epsilon_{r1}}$ and $n_2 = \sqrt{\epsilon_{r2}}$ are the refractive indices of medium 1 and medium 2, respectively and ϵ_{r1} and ϵ_{r2} are the relative permittivities in medium 1 and medium 2, respectively.

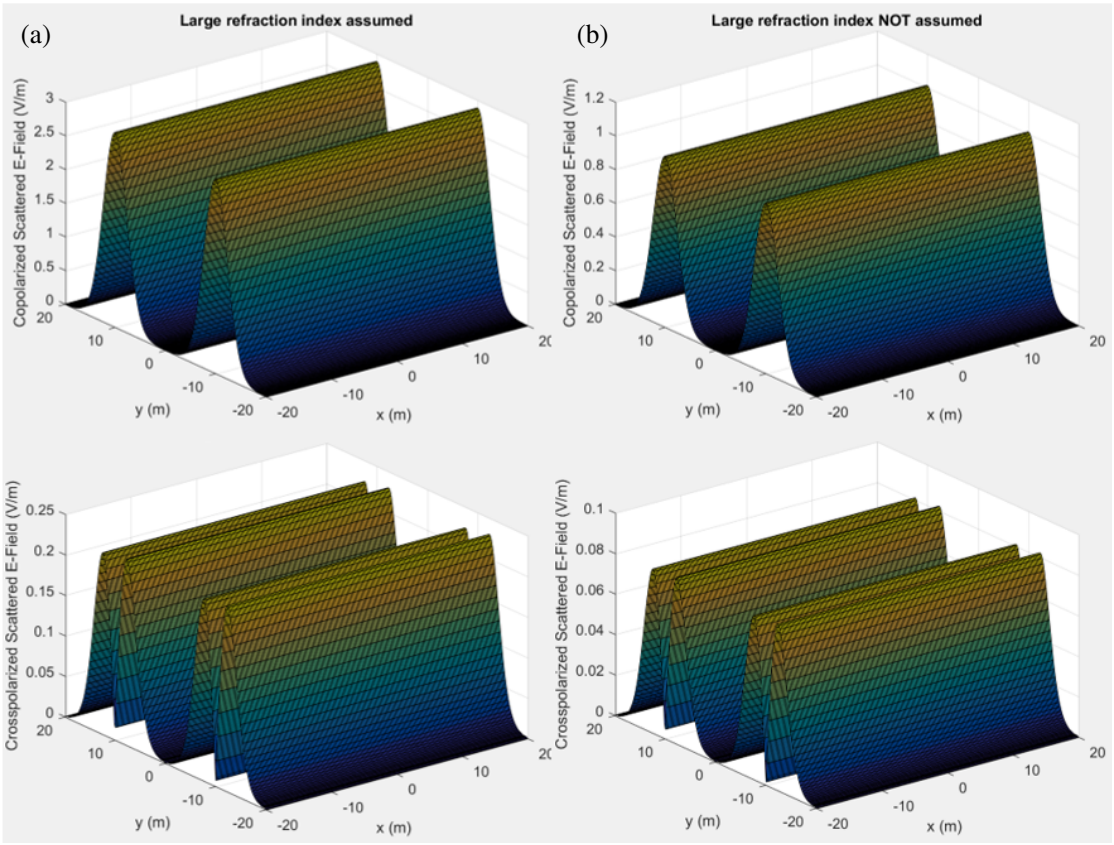

Figure 2. Co (top) and cross (bottom) polarized backscatter terms when the refractive index is assumed to be (a) large and (b) small.

3. STRATIFIED MEDIA SCATTERING

Walsh [17], developed the scattering equations for stratified media using a similar approach as was used for rough surfaces. The equations are developed for a two layer case, as illustrated in Figure 3, and then generalized to any number of layers. The source is assumed to be outside the layers in freespace, each layer is homogeneous with respect to its electrical properties and the interfaces between layers are assumed to be smooth.

Rather than showing the derivation of the equations as was done for the rough surface case, the emphasis will be placed on interpreting the scattering equations. The x component of the total field above the layers may be written for a two layer system as [17]

$$\underline{E}_x^{z^+} = \underline{E}_{sx}^{z^+} + e^{-z^+ u_0} \left[\frac{u_0 - U_{1h}}{u_0 + U_{1h}} \left(\underline{E}_{0sx} - \frac{jk_x u_0}{\lambda^2} \underline{E}_{0sz} \right) - \frac{jk_x u_0}{\lambda^2} \frac{u_0 - \dfrac{1}{n_{01}^2}}{u_0 - \dfrac{1}{n_{01}^2}} \underline{E}_{0sz} \right] \tag{23}$$

where n_{01} is the refractive index for the top layer, and $\underline{E}_{0sx}$ and $\underline{E}_{0sz}$ are the transforms of the x and z components, respectively, of the electric field at $z = 0$. The term u_0 has the same meaning as u for the rough surface scattering equations, but a subscript is added to differentiate the value in each layer and layer 0 is the top layer where the source is located and U_{1h} and U_{1z} are a function of the electrical characteristics of the two layers and are calculated recursively as $U_{1h} = \frac{u_1 \tanh(a_1 u_1) + U_{2h}}{1 + \tanh(a_1 u_1) \frac{U_{2h}}{u_m}}$ and

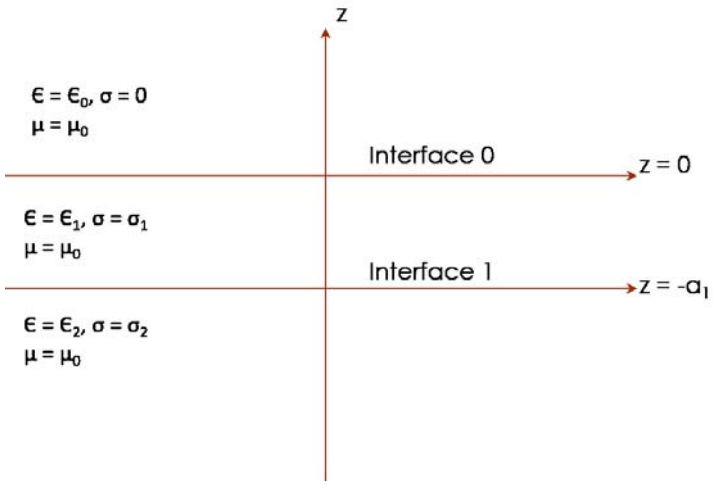

Figure 3. Geometry and parameters for two-layer model.

$U_{1z} = \frac{u_1 \tanh(a_1 u_1) + \frac{n_{01}^2}{n_{02}^2} U_{2z}}{1 + \tanh(a_1 u_1) \frac{n_{01}^2}{n_{02}^2} \frac{U_{2z}}{u_1}}$, where $U_{Mh} = U_{Mz} = u_M$, a_1 is the thickness of the first layer, and N_{10} depends on the relative permittivities of the top layer and free space. The field above the layers given by Eq. (23) consists of a source or zero order scatter term, $\underline{E}_{sx}^{z^+}$, and a scattered term. This relationship is more explicitly obvious when the source is an infinitesimal vertical or horizontal dipole.

For a vertical dipole of differential length, dl, with current I centred at h above the surface, the source current density is specified as $\vec{J}_s = Idl\delta(x)\delta(y)\delta(z-h)\hat{z}$. The z component of the electric field will be dominant for this vertical dipole and the total field above the layers is given as

$$\underline{E}_z^{z^+} = \frac{Idl}{j\omega\epsilon_0}\left(\frac{\partial^2}{\partial z^2} + k^2\right)\left[\frac{e^{-|z^+-h|u_0}}{2u_0} + \frac{e^{-(z^++h)u_0}}{2u_0}\frac{u_0 - \frac{1}{n_{01}^2}U_{1z}}{u_0 + \frac{1}{n_{01}^2}U_{1z}}\right] \tag{24}$$

where the z component of the source, $\underline{E}_{sz}$, is

$$\underline{E}_{sz} = \frac{Idl}{j\omega\epsilon_0}\left(\frac{\partial^2}{\partial z^2} + k^2\right)\left[\frac{e^{-|z-h|u_0}}{2u_0}\right] \tag{25}$$

From Eq. (24) it can be seen that the scattered field is a scaled version of the image of the source where the scale factor is $(u_0 - U_{1z}/n_{01}^2)(u_0 + U_{1z}/n_{01}^2)$. The x and y components of the scattered field exhibit this same structure, which is reminiscent of the Fresnel reflection coefficient for vertically polarized waves. For plane wave incidence, Walsh [15] presents the reflection coefficient for vertical polarization as

$$r_V = \frac{u_0 - k\frac{\sqrt{n_0^2 - 1}}{n_0^2}}{u_0 + k\frac{\sqrt{n_0^2 - 1}}{n_0^2}} \tag{26}$$

Thus, for the vertical dipole, the field scattered from stratified layers can be represented in terms of an effective reflection coefficient. Now let us consider the scattered field from a horizontal dipole assumed, without loss of generality, to be aligned in the x direction at a height h above the surface. The current density is given as $\vec{J}_s = Idl\delta(x)\delta(y)\delta(z-h)\hat{x}$. For propagation through the layers, as for ground penetrating radar applications, the dominant field is in the $\hat{x}$ direction. Thus, we will focus on the x

component of the field above the layers, which can be written as

$$\underline{E}_x^{z^+} = \frac{Idl}{j\omega\epsilon_0}\left[(k^2-k_x^2)\left(\frac{e^{|z^+-h|u_0}}{2u_0}+\frac{u_0-U_{1h}}{u_0+U_{1h}}\frac{e^{(z^++h)u_0}}{2u_0}\right)-jk_xu_0\frac{jk_x(N_{10}+1/n_{01}^2\nu_1)e^{(z^++h)u_0}}{(u_0+U_{1h})(u_0+1/n_{01^2}U_{1z})}\right] \quad (27)$$

where ν_1 is calculated recursively as $\nu_1 = \frac{(1-\tanh^2(a_1u_1))\left(\frac{n_{01}^2}{n_{02}^2}\nu_2+N_{21}\right)}{\left(1+\tanh(a_1u_1)\frac{U_{2h}}{u_1}\right)\left(1+\tanh(a_1u_1)\frac{n_{01}^2}{n_{02}^2}\frac{U_{2z}}{u_1}\right)}$ and $\nu_M = 0$. Unlike for the vertical dipole, there are now three terms in the equation. It can be shown through simulation that the final term is negligible, allowing Eq. (27) to be expressed with the same structure as (24), i.e.,

$$\underline{E}_x^{z^+} \approx \frac{Idl}{j\omega\epsilon_0}\left[(k^2-k_x^2)\left(\frac{e^{|z^+-h|u}}{2u}+\frac{u-U_{1h}}{u+U_{1h}}\frac{e^{(z^++h)u}}{2u}\right)\right]. \quad (28)$$

Removing the negligible term simplifies the inverse Fourier transform and reduces the reliance on numerical integration methods. The field above the layers for the horizontal dipole contains direct and scattered energies. The multiplying factor on the scattered wave bears resemblance to the reflection coefficient for horizontally polarized waves, which can be expressed as

$$r_H = \frac{u-k\frac{n_0^2}{\sqrt{n_0^2-1}}}{u+k\frac{n_0^2}{\sqrt{n_0^2-1}}} \quad (29)$$

4. APPLICATION TO SEA ICE RIDGES

The goal of this research is to model backscatter from sea ice ridges using an aerial-mounted ice penetrating radar. Sea ice ridges are modeled as layered media with a rough surface. Sea ice ridges consist of a sail, consolidated layer and rubble as depicted in Figure 4. The consolidated layer is below the water surface and, combined with the rubble, forms the keel. The keel is usually wider than the sail and extends below the level ice [21]. The sail is the above water portion and tends to be the most porous section with low salinity. The consolidated layer starts off as 1.5 to 2 times the level ice thickness and grows as the ice ages. This is the strongest part of the ridge and it forms as the blocks of ice refreeze together. For ice that survives the first melt season (second year ice) or several melt seasons (multiyear ice) the consolidated layer grows as melt water percolates into pores vacated by brine and refreezes. The keel, which is the underwater portion of the ridge, may be almost fully consolidated for the entire thickness of the keel for multiyear (MY) ridges [22].

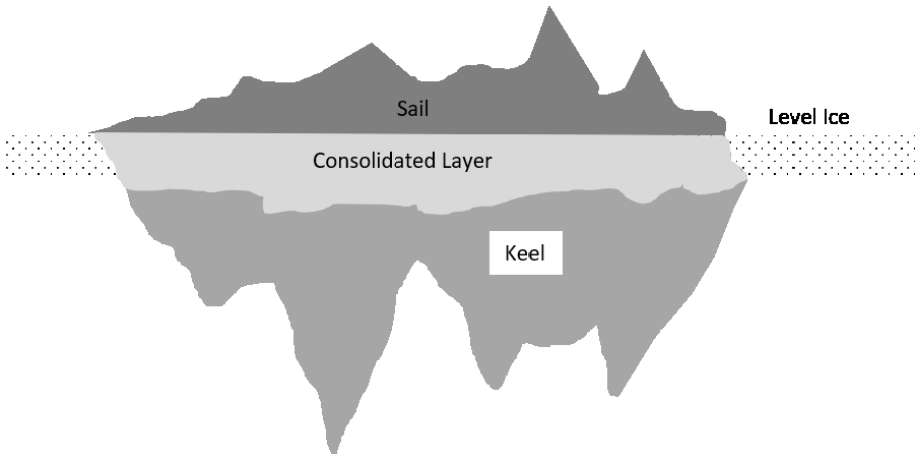

Figure 4. Illustration of main parts of a sea ice ridge.

Ridges form as ice floes collide with each other, with land fast ice or the shoreline. Pressure ridges occur due to compressive forces and the ice fails due to bending [23] or buckling [24]. Ridges are quasi-linear and are found with a range of lengths and are comprised of a range of ice block sizes. The average thickness of the blocks is usually under 0.4 m [25] with lengths two [26] to five [27] times greater than their thickness. Ridges tend to be formed from first year (FY) ice thinner than 50 cm since the driving forces (i.e., winds, currents, waves) are generally not strong enough to ridge fully developed (2 m) FY ice. Shear ridges are formed from shear forces, tend to be linear with lengths up to several kilometers and the ice blocks are more thoroughly crushed [25]. During ridging, the ice in contact gets broken and, while some of it gets pushed upwards, most of it gets pushed downwards due to buoyancy. Individual blocks of ice are visible in newly formed ridges. MY ridges and MY ridged floes have smoother, undulating surfaces.

4.1. Ridges as Rough Surfaces

Surface roughness depends on the nature of the surface variations, the wavelength of the radar energy and the local angle of incidence. Rayleigh suggested that surfaces are smooth when the path difference between incident waves, $\Delta\phi$, is less than $\pi/2$, which corresponds to surface height variations of $\sigma_h < \lambda/8\cos(\theta)$, where θ is the incidence angle of the radar energy. Norton suggested that the choice of $\pi/2$ was arbitrary and that path differences must be within $\pi/4$ [28] or $\pi/8$ [29] for a surface to be considered smooth.

It has been suggested that surface roughness also depends on the separate cases of scattering from the surface or transmission through the surface [19]. As with the Rayleigh and Norton approaches, the criterion for surface roughness depends on the path difference introduced by the surface roughness. The Rayleigh roughness parameter for reflection, Ra_r, and transmission, Ra_t, are used to determine if the surface is smooth, slightly rough or very rough. The incidence angle plays a major role in determining the degree of roughness and a surface which is rough for reflection may be smooth for transmission for one viewing geometry and vice versa for another incidence angle. Surfaces are considered slightly rough for Ra_r, $Ra_t > \pi/16$ and very rough for Ra_r, $Ra_t > \pi/C$, where C is a constant selected between 2 and π. The expressions for the Rayleigh roughness parameter are (as found, for example, in [19])

$$Ra_r = k_1\sigma_h\cos\theta_i$$
$$Ra_t = k_0\sigma_h\frac{|n_1\cos\theta_1 - n_2\cos\theta_t|}{2}.$$

Surface roughness is relevant as it determines the balance between coherent and incoherent scatter. The average intensity of the scattered field, $\left\langle\left|\vec{E}^s\right|^2\right\rangle$, can be expressed as the sum of the coherent, $\left|\langle\vec{E}^s\rangle\right|^2$, and incoherent, $\left|\langle\delta\vec{E}^s\rangle\right|^2$, components. For fully coherent scatter, as from an infinite smooth, flat surface, the scattered field would be dominated by the specular component. For scatter from a very rough surface the incoherent scatter term would dominate and all other cases would have a balance between coherent and incoherent scatter.

Walsh's method, which is the basis for this model development, assumes incoherent scatter from very rough surfaces, but coherent scatter is more likely to occur at normal incidence at short ranges. Since ice penetrating radar would typically operate at normal incidence and at moderate heights above the surface it cannot be assumed that the surface is rough. A simple simulation (see Figure 5) was conducted to verify that it is reasonable to assume ridges are rough for energy reflection and transmission for frequencies ranging from 50 MHz to 500 MHz, which are typically used for penetrating radar applications.

Wadhams [30] has developed an exponential model to describe sail height distributions, but for this analysis full surface details are not needed. Instead, three different roughness scales are considered, to correspond with typical ice block thickness, and lower and upper bounds of typical block length. Roughness scales based on block thickness and the lower limit for block length are consistent with topography measurements made over first year and multiyear ice regimes in the central Arctic and Beaufort/Chukchi Sea areas [31]. The maximum roughness scale used may also correspond to ridge height. It may be noted, for the geometry and surface roughness considered here, the surface is very

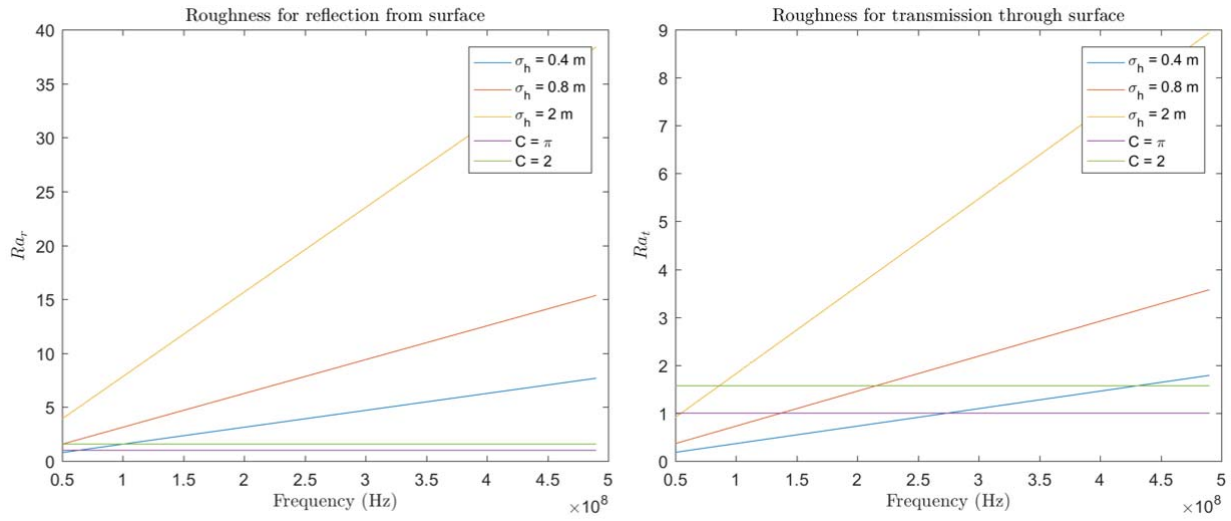

Figure 5. Surface roughness.

rough above 100 MHz for reflection from the surface. For transmission, it can be seen that ice ridges will not be rough based on block thickness until 275 MHz or 425 MHz and that the upper bound for ice block length is needed to have a rough surface for all frequencies above 100 MHz. It is interesting to note that with 0.4 m surface variation, the surface would be considered rough for transmission at 100 MHz using the standard Rayleigh criterion. Care must be taken when applying Walsh's approach since assumptions of small surface height with respect to radar wavelength are often made to simplify the analysis, but this will not be possible for modeling the scatter from sea ice ridges.

4.2. Ridges as Layered Surfaces

Sea ice ridges are created through chaotic processes and cannot be assumed to be stratified with homogeneous properties in each layer. Nonetheless, it is possible to simplify sea ice profiles as being stratified with minimal impact on scattering. Researchers at CRREL [32] collected ice penetrating radar signatures over second year ridges and validated the radar data using ice cores collected at 1 m intervals with ice properties calculated and measured every 0.1 m of depth. For illustration purposes, the salinity and brine volume profiles at one site are shown below in Figure 6. Models to calculate the ice parameters are presented in [33].

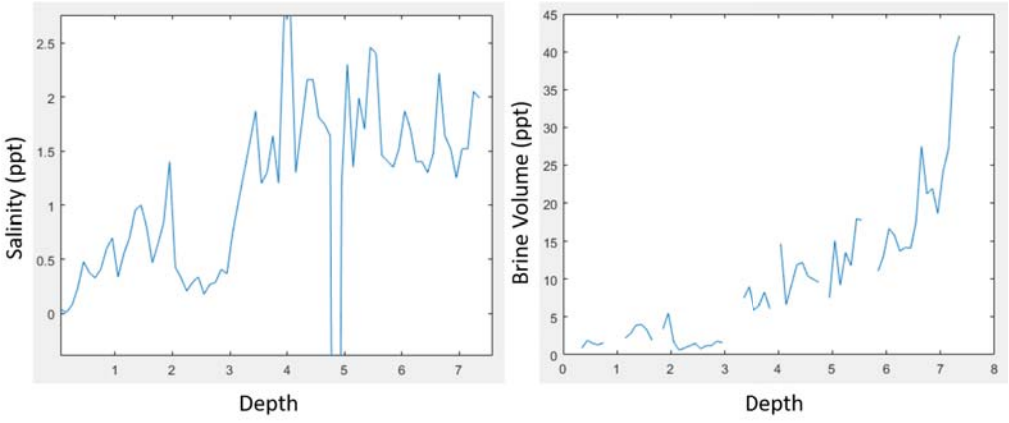

Figure 6. Salinity and Brine volume for a second year ridge.

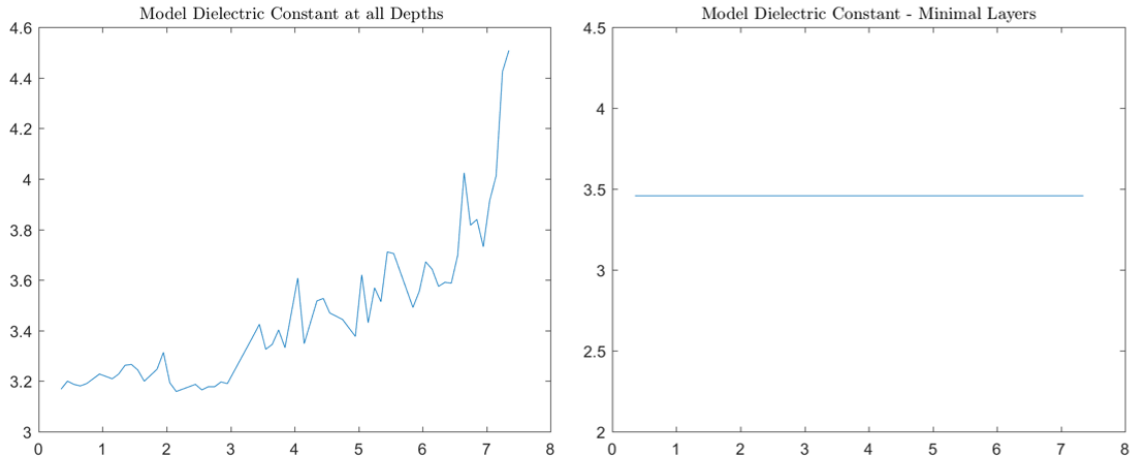

Figure 7. Effective reflections from sea ice ridge.

It is apparent from the salinity profile of Figure 6 that there are three distinct regions. For the first two metres of the ridge, the salinity has a mid-level average value with high variability. From 2 to 3 m the average salinity is low with low variability and the remainder of the ridge has high salinity that is highly variable. At first glance it appears that these three layers correspond to the sail, consolidated layer and rubble, as illustrated in Figure 4, however, the authors do not provide information on the consolidated layer. One additional link between the physical model and the ice properties can be observed from the brine volume plot. Brine volume, which is a calculated quantity, exhibits the same three layers plus an extra layer at the bottom of the ridge where the value rapidly increases. The final layer likely corresponds to the skeletal layer at the ridge bottom. The skeletal layer is a lattice of weak ice a few centimeters thick that undergoes advective transfer with the sea water.

In general, sea ice ridge profiles will be more complex than the data presented in Figure 6. A more robust approach based on variations in the permittivity will be used to define the ice layers. A rough guideline from field studies indicates that a discrete change of approximately 40% in the relative permittivity is required to generate a weak reflection [34]. Assuming a minimum change of 30% in the relative permittivity and applying Eq. (22) corresponds to a reflection coefficient of approximately $\Gamma = 8\%$. Using this criteria for the ridge of Figure 6 results in the ridge appearing as a single layer, as illustrated in Figure 7. An approach developed by Wait [11] can be used to calculate the effective relative permittivity of the layered ridge, which is needed to calculate the scatter from a rough surface. The effective relative permittivity is used, for example, to calculate variants of u_1 in Eq. (21).

Sea ice ridges often have air voids between ice blocks, large brine pockets or unfrozen sea water and partially frozen ice and may be covered in wet or dry snow. Sea ice ridge models will be developed to include these features as extra layers and simulations will reveal the impact they have on the backscatter.

5. CONCLUSIONS AND FUTURE WORK

This paper considers the scattering, at nadir incidence, from sea ice ridges that are modeled as having simple rough surfaces with layers. Scattering equations have been developed for a plane wave over a 1D rough surface with an arbitrary permittivity and it has been shown that the dielectric permittivity of the surface affects only the magnitude of the scatter, since some of the wave energy will be transmitted through the surface when the relative permittivity is not infinite. Justification has been provided to consider sea ice ridges as layered media with a rough surface. The scattering equations for both rough surface and stratified media have been arranged to emphasize that the scattered portion of the wave can be expressed in terms of a scattering coefficient applied to the source or image of the source. Work is currently underway to bring the two elements of the research together and express the field backscattered from layered media with a rough surface using the known scattering coefficients. Work is also underway to model scatter from a general stationary rough surface and extend results to general surface slopes.

REFERENCES

1. Rayleigh, J. W. S. B., *The Theory of Sound*, V.1, Macmillan, 1894.
2. Rice, S. O., "Reflection of electromagnetic waves from slightly rough surfaces," *Communications on Pure and Applied Mathematics*, Vol. 4, No. 2-3, 351–378, 1951.
3. Wait, J. R., "Perturbation analysis for reflection from two-dimensional periodic sea waves," *Radio Science*, Vol. 6, No. 3, 387–391, 1971.
4. Barrick, D. E., "Theory of HF and VHF propagation across the rough sea, 1, the effective surface impedance for a slightly rough highly conducting medium at grazing incidence," *Radio Science*, Vol. 6, No. 5, 517–526, 1971.
5. Barrick, D. E., "Theory of HF and VHF propagation across the rough sea, 2, application to HF and VHF propagation above the sea," *Radio Science*, Vol. 6, No. 5, 527–533, 1971.
6. Rosich, R. K. and J. R. Wait, "A general perturbation solution for reflection from two-dimensional periodic surfaces," *Radio Science*, Vol. 12, No. 5, 719–729, 1977.
7. Rodríguez, E. and Y. Kim, "A unified perturbation expansion for surface scattering," *Radio Science*, Vol. 27, No. 1, 79–93, 1992.
8. Ogilvy, J. A., "Wave scattering from rough surfaces," *Reports on Progress in Physics*, Vol. 50, No. 12, 1553, 1987.
9. Winebrenner, D. P. and A. Ishimaru, "Application of the phase-perturbation technique to randomly rough surfaces," *Journal of the Optical Society of America A*, 1985.
10. Rodríguez, E., "Beyond the Kirchoff plane approximation," *Radio Science*, 1989.
11. Wait, J. R., "Chapter II — Reflection of electromagnetic waves from horizontally stratified media," *Electromagnetic Waves in Stratified Media (Revised Edition Including Supplemented Material)*, J. R. Wait, ed., 8–63, Pergamon, 1970.
12. Tamir, T., H. C. Wang, and A. A. Oliner, "Wave propagation in sinusoidally stratified dielectric media," *IEEE Transactions on Microwave Theory and Techniques*, Vol. 12, 323–335, May 1964.
13. Chen, Y. M., "Wave propagation in stratified random media," *Radio Science*, 1964.
14. Bahar, E., "Radio wave propagation in stratified media with nonuniform boundaries and varying electromagnetic parameters: Full wave analysis," *Canadian Journal of Physics*, 1972.
15. Walsh, J., "On the theory of electromagnetic propagation across a rough surface and calculations in the VHF region," *Tech. Rep.*, Memorial University, 1980.
16. Walsh, J. and S. K. Srivastava, "Rough surface propagation and scatter: 1. General formulation and solution for periodic surfaces," *Radio Science*, 1987.
17. Walsh, J. and R. Donnelly, "A general theory of the interaction of electromagnetic waves with isotropic, horizontally layered media1 (summary)," *Radio Science*, 1987.
18. Walsh, J. and R. Donnelly, "Consolidated approach to two-body electromagnetic scattering," *Physical Review A*, 1987.
19. Pinel, N., C. Bourlier, and J. Saillard, "Degree of roughness of rough layers: Extensions of the rayleigh roughness criterion and some applications," *Progress In Electromagnetic Research*, 2010.
20. Rice, S. O., "Mathematical analysis of random noise," *The Bell System Technical Journal*, Vol. 23, 282–332, July 1944.
21. Strub-Klein, L. and D. Sudom, "A comprehensive analysis of the morphology of first-year sea ice ridges," *Cold Regions Science and Technology*, Vol. 82, No. Supplement C, 94–109, 2012.
22. Kovacs, A., W. F. Weeks, S. Ackley, and W. D. Hibler, "Structure of a multi-year pressure ridge," *ARCTIC*, Vol. 26, No. 1, 1973.
23. Parmerter, R. R. and M. D. Coon, "Model of pressure ridge formation in sea ice," *Journal of Geophysical Research*, Vol. 77, No. 33, 6565–6575, 1972.
24. Kovacs, A. and D. Sodhi, "Ice pile-up and ride-up on arctic and subarctic beaches," *Coastal Engineering*, Vol. 5, No. Supplement C, 247–273, 1981.
25. Tucker, W. B. III, D. S. Sodhi, and J. W. Govoni, "Structure of first-year pressure ridge sails in the Prudhoe bay region," *The Alaskan Beaufort Sea*, P. W. Barnes, D. M. Schell, and E. Reimnitz,

eds., 115–135, Academic Press, 1984.

26. Weeks, W. F., *On Sea Ice*, University of Alaska Press, 2010.
27. Kubat, I., D. Fowler, and M. Sayed, "Chapter 18 — oating ice and ice pressure challenge to ships," *Snow and Ice-related Hazards, Risks and Disasters*, J. F. Shroder, W. Haeberli, and C. Whiteman (eds.), 647–676, Academic Press, Boston, 2015.
28. Norton, K. A. and A. C. Omberg, "Maximum range of a radar set," *Proceedings of the IRE*, 1947.
29. Kerr, D. E., "The propagation of short radio waves," *Tech. Rep.*, MIT Radiation Lab. Series No. 13, 1951.
30. Wadhams, P., "A comparison of sonar and laser profiles along corresponding tracks in the arctic ocean," *Sea Ice Processes and Models*, R. S. Pritchard, ed., 1980.
31. Petty, A. A., M. C. Tsamados, N. T. Kurtz, S. L. Farrell, T. Newman, J. P. Harbeck, D. L. Feltham, and J. A. Richter-Menge, "Characterizing arctic sea ice topography using high-resolution icebridge data," *The Cryosphere*, 2016.
32. Kovacs, A. and R. M. Morey, "Electromagnetic measurements of multi-year sea ice using impulse radar," *Cold Regions Science and Technology*, Vol. 12, No. 1, 67–93, 1986.
33. Morey, R. M., A. Kovacs, and G. F. N. Cox, "Electromagnetic properties of sea ice," *Cold Regions Science and Technology*, Vol. 9, No. 1, 53–75, 1984.
34. GeoScan Ground Penetrating Radar.